Measurement of the $\overline{B}^0$ lifetime and the $B^0\overline{B}^0$ oscillation frequency using partially reconstructed $\overline{B}^0 \to D^{*+}\ell^-\overline{\nu}_\ell$ decays

B. Aubert,[1] R. Barate,[1] D. Boutigny,[1] F. Couderc,[1] Y. Karyotakis,[1] J. P. Lees,[1] V. Poireau,[1] V. Tisserand,[1] A. Zghiche,[1] E. Grauges,[2] A. Palano,[3] M. Pappagallo,[3] A. Pompili,[3] J. C. Chen,[4] N. D. Qi,[4] G. Rong,[4] P. Wang,[4] Y. S. Zhu,[4] G. Eigen,[5] I. Ofte,[5] B. Stugu,[5] G. S. Abrams,[6] M. Battaglia,[6] A. B. Breon,[6] D. N. Brown,[6] J. Button-Shafer,[6] R. N. Cahn,[6] E. Charles,[6] C. T. Day,[6] M. S. Gill,[6] A. V. Gritsan,[6] Y. Groysman,[6] R. G. Jacobsen,[6] R. W. Kadel,[6] J. Kadyk,[6] L. T. Kerth,[6] Yu. G. Kolomensky,[6] G. Kukartsev,[6] G. Lynch,[6] L. M. Mir,[6] P. J. Oddone,[6] T. J. Orimoto,[6] M. Pripstein,[6] N. A. Roe,[6] M. T. Ronan,[6] W. A. Wenzel,[6] M. Barrett,[7] K. E. Ford,[7] T. J. Harrison,[7] A. J. Hart,[7] C. M. Hawkes,[7] S. E. Morgan,[7] A. T. Watson,[7] M. Fritsch,[8] K. Goetzen,[8] T. Held,[8] H. Koch,[8] B. Lewandowski,[8] M. Pelizaeus,[8] K. Peters,[8] T. Schroeder,[8] M. Steinke,[8] J. T. Boyd,[9] J. P. Burke,[9] N. Chevalier,[9] W. N. Cottingham,[9] M. P. Kelly,[9] T. Cuhadar-Donszelmann,[10] B. G. Fulsom,[10] C. Hearty,[10] N. S. Knecht,[10] T. S. Mattison,[10] J. A. McKenna,[10] A. Khan,[11] P. Kyberd,[11] M. Saleem,[11] L. Teodorescu,[11] A. E. Blinov,[12] V. E. Blinov,[12] A. D. Bukin,[12] V. P. Druzhinin,[12] V. B. Golubev,[12] E. A. Kravchenko,[12] A. P. Onuchin,[12] S. I. Serednyakov,[12] Yu. I. Skovpen,[12] E. P. Solodov,[12] A. N. Yushkov,[12] D. Best,[13] M. Bondioli,[13] M. Bruinsma,[13] M. Chao,[13] I. Eschrich,[13] D. Kirkby,[13] A. J. Lankford,[13] M. Mandelkern,[13] R. K. Mommsen,[13] W. Roethel,[13] D. P. Stoker,[13] C. Buchanan,[14] B. L. Hartfiel,[14] A. J. R. Weinstein,[14] S. D. Foulkes,[15] J. W. Gary,[15] O. Long,[15] B. C. Shen,[15] K. Wang,[15] L. Zhang,[15] D. del Re,[16] H. K. Hadavand,[16] E. J. Hill,[16] D. B. MacFarlane,[16] H. P. Paar,[16] S. Rahatlou,[16] V. Sharma,[16] J. W. Berryhill,[17] C. Campagnari,[17] A. Cunha,[17] B. Dahmes,[17] T. M. Hong,[17] M. A. Mazur,[17] J. D. Richman,[17] W. Verkerke,[17] T. W. Beck,[18] A. M. Eisner,[18] C. J. Flacco,[18] C. A. Heusch,[18] J. Kroseberg,[18] W. S. Lockman,[18] G. Nesom,[18] T. Schalk,[18] B. A. Schumm,[18] A. Seiden,[18] P. Spradlin,[18] D. C. Williams,[18] M. G. Wilson,[18] J. Albert,[19] E. Chen,[19] G. P. Dubois-Felsmann,[19] A. Dvoretskii,[19] D. G. Hitlin,[19] I. Narsky,[19] T. Piatenko,[19] F. C. Porter,[19] A. Ryd,[19] A. Samuel,[19] R. Andreassen,[20] S. Jayatilleke,[20] G. Mancinelli,[20] B. T. Meadows,[20] M. D. Sokoloff,[20] F. Blanc,[21] P. Bloom,[21] S. Chen,[21] W. T. Ford,[21] U. Nauenberg,[21] A. Olivas,[21] P. Rankin,[21] W. O. Ruddick,[21] J. G. Smith,[21] K. A. Ulmer,[21] S. R. Wagner,[21] J. Zhang,[21] A. Chen,[22] E. A. Eckhart,[22] A. Soffer,[22] W. H. Toki,[22] R. J. Wilson,[22] Q. Zeng,[22] D. Altenburg,[23] E. Feltresi,[23] A. Hauke,[23] B. Spaan,[23] T. Brandt,[24] J. Brose,[24] M. Dickopp,[24] V. Klose,[24] H. M. Lacker,[24] R. Nogowski,[24] S. Otto,[24] A. Petzold,[24] G. Schott,[24] J. Schubert,[24] K. R. Schubert,[24] R. Schwierz,[24] J. E. Sundermann,[24] D. Bernard,[25] G. R. Bonneaud,[25] P. Grenier,[25] S. Schrenk,[25] Ch. Thiebaux,[25] G. Vasileiadis,[25] M. Verderi,[25] D. J. Bard,[26] P. J. Clark,[26] W. Gradl,[26] F. Muheim,[26] S. Playfer,[26] Y. Xie,[26] M. Andreotti,[27] V. Azzolini,[27] D. Bettoni,[27] C. Bozzi,[27] R. Calabrese,[27] G. Cibinetto,[27] E. Luppi,[27] M. Negrini,[27] L. Piemontese,[27] F. Anulli,[28] R. Baldini-Ferroli,[28] A. Calcaterra,[28] R. de Sangro,[28] G. Finocchiaro,[28] P. Patteri,[28] I. M. Peruzzi,[28,*] M. Piccolo,[28] A. Zallo,[28] A. Buzzo,[29] R. Capra,[29] R. Contri,[29] M. Lo Vetere,[29] M. Macri,[29] M. R. Monge,[29] S. Passaggio,[29] C. Patrignani,[29] E. Robutti,[29] A. Santroni,[29] S. Tosi,[29] S. Bailey,[30] G. Brandenburg,[30] K. S. Chaisanguanthum,[30] M. Morii,[30] E. Won,[30] J. Wu,[30] R. S. Dubitzky,[31] U. Langenegger,[31] J. Marks,[31] S. Schenk,[31] U. Uwer,[31] W. Bhimji,[32] D. A. Bowerman,[32] P. D. Dauncey,[32] U. Egede,[32] R. L. Flack,[32] J. R. Gaillard,[32] G. W. Morton,[32] J. A. Nash,[32] M. B. Nikolich,[32] G. P. Taylor,[32] W. P. Vazquez,[32] M. J. Charles,[33] W. F. Mader,[33] U. Mallik,[33] A. K. Mohapatra,[33] J. Cochran,[34] H. B. Crawley,[34] V. Eyges,[34] W. T. Meyer,[34] S. Prell,[34] E. I. Rosenberg,[34] A. E. Rubin,[34] J. Yi,[34] N. Arnaud,[35] M. Davier,[35] X. Giroux,[35] G. Grosdidier,[35] A. Höcker,[35] F. Le Diberder,[35] V. Lepeltier,[35] A. M. Lutz,[35] A. Oyanguren,[35] T. C. Petersen,[35] M. Pierini,[35] S. Plaszczynski,[35] S. Rodier,[35] P. Roudeau,[35] M. H. Schune,[35] A. Stocchi,[35] G. Wormser,[35] C. H. Cheng,[36] D. J. Lange,[36] M. C. Simani,[36] D. M. Wright,[36] A. J. Bevan,[37] C. A. Chavez,[37] J. P. Coleman,[37] I. J. Forster,[37] J. R. Fry,[37] E. Gabathuler,[37] R. Gamet,[37] K. A. George,[37] D. E. Hutchcroft,[37] R. J. Parry,[37] D. J. Payne,[37] K. C. Schofield,[37] C. Touramanis,[37] C. M. Cormack,[38] F. Di Lodovico,[38] R. Sacco,[38] C. L. Brown,[39] G. Cowan,[39] H. U. Flaecher,[39] M. G. Green,[39] D. A. Hopkins,[39] P. S. Jackson,[39] T. R. McMahon,[39] S. Ricciardi,[39] F. Salvatore,[39] D. Brown,[40] C. L. Davis,[40] J. Allison,[41] N. R. Barlow,[41] R. J. Barlow,[41] M. C. Hodgkinson,[41] G. D. Lafferty,[41] M. T. Naisbit,[41] J. C. Williams,[41] C. Chen,[42] A. Farbin,[42] W. D. Hulsbergen,[42] A. Jawahery,[42] D. Kovalskyi,[42] C. K. Lae,[42] V. Lillard,[42] D. A. Roberts,[42] G. Simi,[42] G. Blaylock,[43] C. Dallapiccola,[43] S. S. Hertzbach,[43] R. Kofler,[43] V. B. Koptchev,[43] X. Li,[43] T. B. Moore,[43] S. Saremi,[43] H. Staengle,[43] S. Willocq,[43] R. Cowan,[44] K. Koeneke,[44] G. Sciolla,[44] S. J. Sekula,[44] M. Spitznagel,[44] F. Taylor,[44] R. K. Yamamoto,[44] H. Kim,[45] P. M. Patel,[45] S. H. Robertson,[45] A. Lazzaro,[46] V. Lombardo,[46] F. Palombo,[46] J. M. Bauer,[47] L. Cremaldi,[47] V. Eschenburg,[47] R. Godang,[47] R. Kroeger,[47] J. Reidy,[47] D. A. Sanders,[47] D. J. Summers,[47] H. W. Zhao,[47] S. Brunet,[48] D. Côté,[48] P. Taras,[48] B. Viaud,[48] H. Nicholson,[49] N. Cavallo,[50,†] G. De Nardo,[50] F. Fabozzi,[50,†] C. Gatto,[50] L. Lista,[50] D. Monorchio,[50] P. Paolucci,[50] D. Piccolo,[50] C. Sciacca,[50] M. Baak,[51] H. Bulten,[51] G. Raven,[51] H. L. Snoek,[51] L. Wilden,[51] C. P. Jessop,[52] J. M. LoSecco,[52] T. Allmendinger,[53] G. Benelli,[53] K. K. Gan,[53] K. Honscheid,[53] D. Hufnagel,[53]

P. D. Jackson,[53] H. Kagan,[53] R. Kass,[53] T. Pulliam,[53] A. M. Rahimi,[53] R. Ter-Antonyan,[53] Q. K. Wong,[53] J. Brau,[54] R. Frey,[54] O. Igonkina,[54] M. Lu,[54] C. T. Potter,[54] N. B. Sinev,[54] D. Strom,[54] J. Strube,[54] E. Torrence,[54] A. Dorigo,[55] F. Galeazzi,[55] M. Margoni,[55] M. Morandin,[55] M. Posocco,[55] M. Rotondo,[55] F. Simonetto,[55] R. Stroili,[55] C. Voci,[55] M. Benayoun,[56] H. Briand,[56] J. Chauveau,[56] P. David,[56] L. Del Buono,[56] Ch. de la Vaissière,[56] O. Hamon,[56] M. J. J. John,[56] Ph. Leruste,[56] J. Malclès,[56] J. Ocariz,[56] L. Roos,[56] G. Therin,[56] P. K. Behera,[57] L. Gladney,[57] Q. H. Guo,[57] J. Panetta,[57] M. Biasini,[58] R. Covarelli,[58] S. Pacetti,[58] M. Pioppi,[58] C. Angelini,[59] G. Batignani,[59] S. Bettarini,[59] F. Bucci,[59] G. Calderini,[59] M. Carpinelli,[59] R. Cenci,[59] F. Forti,[59] M. A. Giorgi,[59] A. Lusiani,[59] G. Marchiori,[59] M. Morganti,[59] N. Neri,[59] E. Paoloni,[59] M. Rama,[59] G. Rizzo,[59] J. Walsh,[59] M. Haire,[60] D. Judd,[60] D. E. Wagoner,[60] J. Biesiada,[61] N. Danielson,[61] P. Elmer,[61] Y. P. Lau,[61] C. Lu,[61] J. Olsen,[61] A. J. S. Smith,[61] A. V. Telnov,[61] F. Bellini,[62] G. Cavoto,[62] A. D'Orazio,[62] E. Di Marco,[62] R. Faccini,[62] F. Ferrarotto,[62] F. Ferroni,[62] M. Gaspero,[62] L. Li Gioi,[62] M. A. Mazzoni,[62] S. Morganti,[62] G. Piredda,[62] F. Polci,[62] F. Safai Tehrani,[62] C. Voena,[62] H. Schröder,[63] G. Wagner,[63] R. Waldi,[63] T. Adye,[64] N. De Groot,[64] B. Franek,[64] G. P. Gopal,[64] E. O. Olaiya,[64] F. F. Wilson,[64] R. Aleksan,[65] S. Emery,[65] A. Gaidot,[65] S. F. Ganzhur,[65] P.-F. Giraud,[65] G. Graziani,[65] G. Hamel de Monchenault,[65] W. Kozanecki,[65] M. Legendre,[65] G. W. London,[65] B. Mayer,[65] G. Vasseur,[65] Ch. Yèche,[65] M. Zito,[65] M. V. Purohit,[66] A. W. Weidemann,[66] J. R. Wilson,[66] F. X. Yumiceva,[66] T. Abe,[67] M. T. Allen,[67] D. Aston,[67] R. Bartoldus,[67] N. Berger,[67] A. M. Boyarski,[67] O. L. Buchmueller,[67] R. Claus,[67] M. R. Convery,[67] M. Cristinziani,[67] J. C. Dingfelder,[67] D. Dong,[67] J. Dorfan,[67] D. Dujmic,[67] W. Dunwoodie,[67] S. Fan,[67] R. C. Field,[67] T. Glanzman,[67] S. J. Gowdy,[67] T. Hadig,[67] V. Halyo,[67] C. Hast,[67] T. Hryn'ova,[67] W. R. Innes,[67] M. H. Kelsey,[67] P. Kim,[67] M. L. Kocian,[67] D. W. G. S. Leith,[67] J. Libby,[67] S. Luitz,[67] V. Luth,[67] H. L. Lynch,[67] H. Marsiske,[67] R. Messner,[67] D. R. Muller,[67] C. P. O'Grady,[67] V. E. Ozcan,[67] A. Perazzo,[67] M. Perl,[67] B. N. Ratcliff,[67] A. Roodman,[67] A. A. Salnikov,[67] R. H. Schindler,[67] J. Schwiening,[67] A. Snyder,[67] J. Stelzer,[67] D. Su,[67] M. K. Sullivan,[67] K. Suzuki,[67] S. Swain,[67] J. M. Thompson,[67] J. Va'vra,[67] M. Weaver,[67] W. J. Wisniewski,[67] M. Wittgen,[67] D. H. Wright,[67] A. K. Yarritu,[67] K. Yi,[67] C. C. Young,[67] P. R. Burchat,[68] A. J. Edwards,[68] S. A. Majewski,[68] B. A. Petersen,[68] C. Roat,[68] M. Ahmed,[69] S. Ahmed,[69] M. S. Alam,[69] J. A. Ernst,[69] M. A. Saeed,[69] F. R. Wappler,[69] S. B. Zain,[69] W. Bugg,[70] M. Krishnamurthy,[70] S. M. Spanier,[70] R. Eckmann,[71] J. L. Ritchie,[71] A. Satpathy,[71] R. F. Schwitters,[71] J. M. Izen,[72] I. Kitayama,[72] X. C. Lou,[72] S. Ye,[72] F. Bianchi,[73] M. Bona,[73] F. Gallo,[73] D. Gamba,[73] M. Bomben,[74] L. Bosisio,[74] C. Cartaro,[74] F. Cossutti,[74] G. Della Ricca,[74] S. Dittongo,[74] S. Grancagnolo,[74] L. Lanceri,[74] L. Vitale,[74] F. Martinez-Vidal,[75] R. S. Panvini,[76,‡] Sw. Banerjee,[77] B. Bhuyan,[77] C. M. Brown,[77] D. Fortin,[77] K. Hamano,[77] R. Kowalewski,[77] J. M. Roney,[77] R. J. Sobie,[77] J. J. Back,[78] P. F. Harrison,[78] T. E. Latham,[78] G. B. Mohanty,[78] H. R. Band,[79] X. Chen,[79] B. Cheng,[79] S. Dasu,[79] M. Datta,[79] A. M. Eichenbaum,[79] K. T. Flood,[79] M. Graham,[79] J. J. Hollar,[79] J. R. Johnson,[79] P. E. Kutter,[79] H. Li,[79] R. Liu,[79] B. Mellado,[79] A. Mihalyi,[79] Y. Pan,[79] R. Prepost,[79] P. Tan,[79] J. H. von Wimmersperg-Toeller,[79] S. L. Wu,[79] Z. Yu,[79] and H. Neal[80]

(*BABAR* Collaboration)

[1]*Laboratoire de Physique des Particules, F-74941 Annecy-le-Vieux, France*
[2]*IFAE, Universitat Autonoma de Barcelona, E-08193 Bellaterra, Barcelona, Spain*
[3]*Dipartimento di Fisica and INFN, Università di Bari, I-70126 Bari, Italy*
[4]*Institute of High Energy Physics, Beijing 100039, China*
[5]*Institute of Physics, University of Bergen, N-5007 Bergen, Norway*
[6]*Lawrence Berkeley National Laboratory and University of California, Berkeley, California 94720, USA*
[7]*University of Birmingham, Birmingham, B15 2TT, United Kingdom*
[8]*Institut für Experimentalphysik 1, Ruhr Universität Bochum, D-44780 Bochum, Germany*
[9]*University of Bristol, Bristol BS8 1TL, United Kingdom*
[10]*University of British Columbia, Vancouver, British Columbia, Canada V6T 1Z1*
[11]*Brunel University, Uxbridge, Middlesex UB8 3PH, United Kingdom*
[12]*Budker Institute of Nuclear Physics, Novosibirsk 630090, Russia*
[13]*University of California at Irvine, Irvine, California 92697, USA*
[14]*University of California at Los Angeles, Los Angeles, California 90024, USA*
[15]*University of California at Riverside, Riverside, California 92521, USA*
[16]*University of California at San Diego, La Jolla, California 92093, USA*
[17]*University of California at Santa Barbara, Santa Barbara, California 93106, USA*
[18]*University of California at Santa Cruz, Institute for Particle Physics, Santa Cruz, California 95064, USA*
[19]*California Institute of Technology, Pasadena, California 91125, USA*
[20]*University of Cincinnati, Cincinnati, Ohio 45221, USA*

[21]*University of Colorado, Boulder, Colorado 80309, USA*
[22]*Colorado State University, Fort Collins, Colorado 80523, USA*
[23]*Institut fur Physik, Universität Dortmund, D-44221 Dortmund, Germany*
[24]*Institut für Kern- und Teilchenphysik, Technische Universität Dresden, D-01062 Dresden, Germany*
[25]*Ecole Polytechnique, LLR, F-91128 Palaiseau, France*
[26]*University of Edinburgh, Edinburgh EH9 3JZ, United Kingdom*
[27]*Dipartimento di Fisica and INFN, Università di Ferrara, I-44100 Ferrara, Italy*
[28]*Laboratori Nazionali di Frascati dell'INFN, I-00044 Frascati, Italy*
[29]*Dipartimento di Fisica and INFN, Università di Genova, I-16146 Genova, Italy*
[30]*Harvard University, Cambridge, Massachusetts 02138, USA*
[31]*Physikalisches Institut, Universität Heidelberg, Philosophenweg 12, D-69120 Heidelberg, Germany*
[32]*Imperial College London, London, SW7 2AZ, United Kingdom*
[33]*University of Iowa, Iowa City, Iowa 52242, USA*
[34]*Iowa State University, Ames, Iowa 50011-3160, USA*
[35]*Laboratoire de l'Accélérateur Linéaire, F-91898 Orsay, France*
[36]*Lawrence Livermore National Laboratory, Livermore, California 94550, USA*
[37]*University of Liverpool, Liverpool L69 72E, United Kingdom*
[38]*Queen Mary, University of London, E1 4NS, United Kingdom*
[39]*Royal Holloway and Bedford New College, University of London, Egham, Surrey TW20 0EX, United Kingdom*
[40]*University of Louisville, Louisville, Kentucky 40292, USA*
[41]*University of Manchester, Manchester M13 9PL, United Kingdom*
[42]*University of Maryland, College Park, Maryland 20742, USA*
[43]*University of Massachusetts, Amherst, Massachusetts 01003, USA*
[44]*Laboratory for Nuclear Science, Massachusetts Institute of Technology, Cambridge, Massachusetts 02139, USA*
[45]*McGill University, Montréal, Quebec, Canada H3A 2T8*
[46]*Dipartimento di Fisica and INFN, Università di Milano, I-20133 Milano, Italy*
[47]*University of Mississippi, University, Mississippi 38677, USA*
[48]*Laboratoire René J. A. Lévesque, Université de Montréal, Montréal, Quebec, Canada H3C 3J7*
[49]*Mount Holyoke College, South Hadley, Massachusetts 01075, USA*
[50]*Dipartimento di Scienze Fisiche and INFN, Università di Napoli Federico II, I-80126, Napoli, Italy*
[51]*National Institute for Nuclear Physics and High Energy Physics, NIKHEF, NL-1009 DB Amsterdam, The Netherlands*
[52]*University of Notre Dame, Notre Dame, Indiana 46556, USA*
[53]*The Ohio State University, Columbus, Ohio 43210, USA*
[54]*University of Oregon, Eugene, Oregon 97403, USA*
[55]*Dipartimento di Fisica and INFN, Università di Padova, I-35131 Padova, Italy*
[56]*Laboratoire de Physique Nucléaire et de Hautes Energies, Universités Paris VI et VII, F-75252 Paris, France*
[57]*University of Pennsylvania, Philadelphia, Pennsylvania 19104, USA*
[58]*Dipartimento di Fisica and INFN, Università di Perugia, I-06100 Perugia, Italy*
[59]*Dipartimento di Fisica, Scuola Normale Superiore and INFN, Università di Pisa, I-56127 Pisa, Italy*
[60]*Prairie View A&M University, Prairie View, Texas 77446, USA*
[61]*Princeton University, Princeton, New Jersey 08544, USA*
[62]*Dipartimento di Fisica and INFN, Università di Roma La Sapienza, I-00185 Roma, Italy*
[63]*Universität Rostock, D-18051 Rostock, Germany*
[64]*Rutherford Appleton Laboratory, Chilton, Didcot, Oxon, OX11 0QX, United Kingdom*
[65]*CEA/Saclay, DSM/Dapnia, F-91191 Gif-sur-Yvette, France*
[66]*University of South Carolina, Columbia, South Carolina 29208, USA*
[67]*Stanford Linear Accelerator Center, Stanford, California 94309, USA*
[68]*Stanford University, Stanford, California 94305-4060, USA*
[69]*State University of New York, Albany, New York 12222, USA*
[70]*University of Tennessee, Knoxville, Tennessee 37996, USA*
[71]*University of Texas at Austin, Austin, Texas 78712, USA*
[72]*University of Texas at Dallas, Richardson, Texas 75083, USA*
[73]*Dipartimento di Fisica Sperimentale and INFN, Università di Torino, I-10125 Torino, Italy*
[74]*Dipartimento di Fisica and INFN, Università di Trieste, I-34127 Trieste, Italy*
[75]*IFIC, Universitat de Valencia-CSIC, E-46071 Valencia, Spain*
[76]*Vanderbilt University, Nashville, Tennessee 37235, USA*
[77]*University of Victoria, Victoria, British Columbia, Canada V8W 3P6*
[78]*Department of Physics, University of Warwick, Coventry CV4 7AL, United Kingdom*
[79]*University of Wisconsin, Madison, Wisconsin 53706, USA*
[80]*Yale University, New Haven, Connecticut 06511, USA*
(Received 12 July 2005; published 23 January 2006)

We present a simultaneous measurement of the $\overline{B}^0$ lifetime τ_{B^0} and $B^0\overline{B}^0$ oscillation frequency Δm_d. We use a sample of about 50 000 partially reconstructed $\overline{B}^0 \to D^{*+}\ell^-\bar{\nu}_\ell$ decays identified with the *BABAR* detector at the PEP-II e^+e^- storage ring at SLAC. The flavor of the other B meson in the event is determined from the charge of another high-momentum lepton. The results are $\tau_{B^0} = (1.504 \pm 0.013(\text{stat})^{+0.018}_{-0.013}(\text{syst}))$ ps, $\Delta m_d = (0.511 \pm 0.007(\text{stat})^{+0.007}_{-0.006}(\text{syst}))$ ps^{-1}.

DOI: 10.1103/PhysRevD.73.012004 PACS numbers: 13.25.Hw, 11.30.Er, 12.15.Hh, 14.40.Nd

I. INTRODUCTION

The time evolution of $\overline{B}^0$ mesons is governed by the overall decay rate $\Gamma(\overline{B}^0) = 1/\tau_{B^0}$ and by the mass difference Δm_d of the two mass eigenstates. A precise determination of $\Gamma(\overline{B}^0)$ reduces the systematic error on the parameter $|V_{cb}|$ of the Cabibbo-Kobayashi-Maskawa quark mixing matrix [1]. The parameter $|V_{td}V_{tb}^*|$ enters the box diagram that is responsible for $B^0\overline{B}^0$ oscillations and can be determined from a measurement of Δm_d, although with sizable theoretical uncertainties.

We present a measurement of τ_{B^0} and Δm_d using $\overline{B}^0 \to D^{*+}\ell^-\bar{\nu}_\ell$ decays [2] selected from a sample of about 88×10^6 $B\overline{B}$ events recorded by the *BABAR* detector at the PEP-II asymmetric-energy e^+e^- storage ring, operated at or near the $\Upsilon(4S)$ resonance. $B\overline{B}$ pairs from the $\Upsilon(4S)$ decay move along the beam axis with a nominal Lorentz boost $\langle\beta\gamma\rangle = 0.56$, so that the vertices from the two B decay points are separated on average by about 260 μm. The $B^0\overline{B}^0$ system is produced in a coherent P-wave state, so that flavor oscillation is measurable only relative to the decay of the first B meson. Mixed (unmixed) events are selected by the observation of two equal (opposite) flavor B meson decays. The probabilities of observing mixed (S^-) or unmixed (S^+) events as a function of the proper time difference Δt between decays are

$$S^{\pm}(\Delta t) = \frac{e^{-|\Delta t|/\tau_{B^0}}}{4\tau_{B^0}}(1 \pm \mathcal{D}\cos(\Delta m_d \Delta t)), \qquad (1)$$

where the dilution factor $\mathcal{D}$ is related to the fraction w of events with wrong flavor assignment by the relation $\mathcal{D} = 1 - 2w$ and Δt is computed from the distance between the two vertices projected along the beam direction.

II. THE *BABAR* DETECTOR AND DATA SET

We have analyzed a data sample of 81 fb^{-1} collected by *BABAR* on the $\Upsilon(4S)$ resonance, a sample of 9.6 fb^{-1} collected 40 MeV below the resonance to study the continuum background, and a sample of simulated $B\overline{B}$ events corresponding to about 3 times the size of the data sample. The simulated events are processed through the same analysis chain as the real data. *BABAR* is a multipurpose detector, described in detail in Ref. [3]. The momentum of charged particles is measured by the tracking system, which consists of a silicon vertex tracker (SVT) and a drift chamber (DCH) in a 1.5-T magnetic field. The positions of points along the trajectories of charged tracks measured with the SVT are used for vertex reconstruction and for measuring the momentum of charged particles, including those particles with low transverse momentum that do not reach the DCH due to bending in the magnetic field. The energy loss in the SVT is used to discriminate low-momentum pions from electrons. Higher-energy electrons are identified from the ratio of the energy of their associated shower in the electromagnetic calorimeter (EMC) to their momentum, the transverse profile of the shower, the energy loss in the DCH, and the information from the Cherenkov detector (DIRC). The electron identification efficiency is about 90%, and the hadron misidentification probability is less than 1%. Muons are identified on the basis of the energy deposited in the EMC and the penetration in the instrumented flux return (IFR) of the superconducting coil, which contains resistive plate chambers interspersed with iron. Muon candidates compatible with the kaon hypothesis in the DIRC are rejected. The muon identification efficiency is about 60%, and the hadron misidentification rate is about 2%.

III. ANALYSIS METHOD

A. Selection of $\overline{B}^0 \to D^{*+}\ell^-\bar{\nu}_\ell$ decays

We select events that have more than four charged tracks. We reduce the contamination from light-quark production in continuum events by requiring the normalized Fox-Wolfram second moment [4] to be less than 0.5. We select $\overline{B}^0 \to D^{*+}\ell^-\bar{\nu}_\ell$ events with partial reconstruction of the decay $D^{*+} \to \pi_s^+ D^0$, using only the charged lepton from the $\overline{B}^0$ decay and the soft pion (π_s^+) from the D^{*+} decay. The D^0 decay is not reconstructed, resulting in high selection efficiency. *BABAR* has already published two measurements of τ_{B^0} [5,6] and a measurement of $\sin(2\beta + \gamma)$ [7] based on partial reconstruction of B decays. This technique was originally applied to $\overline{B}^0 \to D^{*+}\ell^-\bar{\nu}_\ell$ decays by ARGUS [8], and then used by CLEO [9], DELPHI [10], and OPAL [11].

To suppress leptons from several background sources, we use only high-momentum leptons, in the range

*Also with Università di Perugia, Dipartimento di Fisica, Perugia, Italy.

†Also with Università della Basilicata, Potenza, Italy.

‡Deceased.

$1.3 < p_\ell < 2.4$ GeV/c [12]. The π_s^+ candidates have momenta ($p_{\pi_s^+}$) between 60 and 200 MeV/c. Because of the limited phase space available in the D^{*+} decay, the π_s^+ is emitted within an approximately one-radian half-opening-angle cone centered about the D^{*+} flight direction. We approximate the direction of the D^{*+} to be that of the π_s^+ and estimate the energy $\tilde{E}_{D^{*+}}$ of the D^{*+} as a function of the energy of the π_s^+ using a third-order polynomial, with parameters taken from the simulation. We define the square of the missing neutrino mass as

$$\mathcal{M}_\nu^2 = \left(\frac{\sqrt{s}}{2} - \tilde{E}_{D^{*+}} - E_{\ell^-}\right)^2 - (\tilde{\mathbf{p}}_{D^{*+}} + \mathbf{p}_{\ell^-})^2, \qquad (2)$$

where we neglect the momentum of the $\overline{B}^0$ in the $\Upsilon(4S)$ frame (on average, 0.34 GeV/c), and identify the $\overline{B}^0$ energy with the beam energy $\sqrt{s}/2$ in the e^+e^- center-of-mass frame. E_{ℓ^-} and $\mathbf{p}_{\ell^-}$ are the energy and momentum vector of the lepton and $\tilde{\mathbf{p}}_{D^{*+}}$ is the estimated momentum vector of the D^{*+}. The distribution of $\mathcal{M}_\nu^2$ peaks at zero for signal events, while it is spread over a wide range for background events (see Fig. 1).

We determine the $\overline{B}^0$ decay point from a vertex fit of the ℓ^- and π_s^+ tracks, constrained to the beam-spot position in the plane perpendicular to the beam axis (the x-y plane). The beam-spot position and size are determined on a run-by-run basis using two-prong events [3]. Its size in the horizontal (x) direction is on average 120 μm. Although the beam-spot size in the vertical (y) direction is only 5.6 μm, we use a constraint of 50 μm in the vertex fit to account for the flight distance of the $\overline{B}^0$ in the x-y plane. We reject events for which the χ^2 probability of the vertex fit, $\mathcal{P}_V$, is less than 0.1%.

We then apply a selection criterion to a combined signal likelihood, $\mathcal{X}$, calculated from p_{ℓ^-}, $p_{\pi_s^+}$, and $\mathcal{P}_V$, which results in a signal-to-background ratio of about one in the signal region defined as $\mathcal{M}_\nu^2 > -2.5$ GeV$^2/c^4$. We reject events for which $\mathcal{X}$ is lower than 0.4 (see Fig. 2). Figure 1 shows the distribution of $\mathcal{M}_\nu^2$ after this selection. The distributions in the top part of the figure are obtained from events in which the ℓ and the π_s have opposite charges (''right charge''), and the distributions in the bottom are from events in which the ℓ and the π_s have equal charges (''wrong charge'').

The points in Fig. 1 correspond to on-resonance data. The dark histograms correspond to off-resonance data, scaled by the ratio of on-resonance to off-resonance integrated luminosity. The hatched histograms correspond to $B\overline{B}$ combinatorial background from simulation. To normalize the $B\overline{B}$ combinatorial background, we scale the $B\overline{B}$ Monte Carlo histogram so that, when added to the luminosity-scaled off-resonance histogram, the sum matches the on-resonance data in the region $\mathcal{M}_\nu^2 < -4.5$ GeV$^2/c^4$. The right-charge plot is shown for illustration only. We use the wrong-charge samples as a cross check to verify that the $B\overline{B}$ combinatorial background shape is described by the simulation. For this purpose, we compare the number of wrong-charge events in the

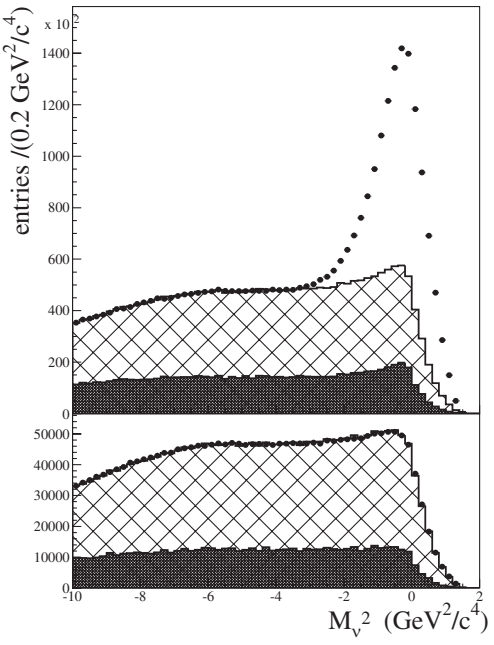

FIG. 1. $\mathcal{M}_\nu^2$ distribution for right-charge (top) and wrong-charge (bottom) events. The points correspond to on-resonance data. The distributions of continuum events (dark histogram), obtained from luminosity-rescaled off-resonance events, and $B\overline{B}$ combinatorial background events (hatched area), obtained from the simulation, are overlaid. Monte Carlo events are normalized to the difference between on-peak and rescaled off-peak data in the region $\mathcal{M}_\nu^2 < -4.5$ GeV$^2/c^4$.

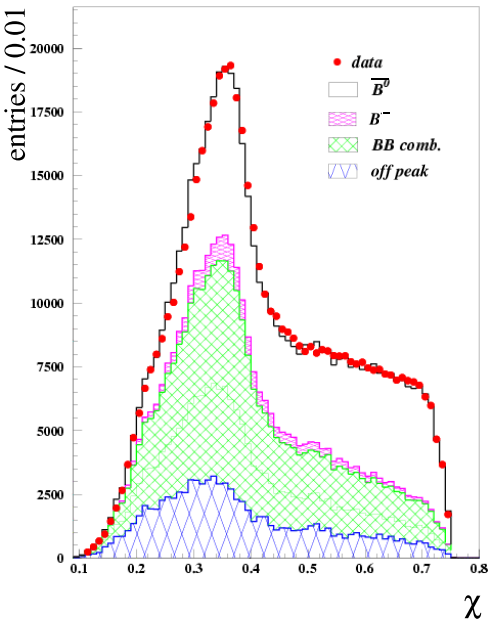

FIG. 2 (color online). Distribution of the combined signal likelihood $\mathcal{X}$ for events in the signal $\mathcal{M}_\nu^2$ region. Events for which $\mathcal{X} < 0.4$ are rejected.

signal region predicted from the sum of off-resonance and $B\overline{B}$ Monte Carlo, normalized as above, to the number of wrong-charge on-resonance data events. This ratio is 0.996 ± 0.002, consistent with unity. For the rest of the analysis we consider only right-charge events.

B. Tag vertex and B flavor tagging

To measure Δm_d we need to know the flavor of both B mesons at their time of decay and their proper decay time difference Δt. The flavor of the partially reconstructed B is determined from the charge of the high-momentum lepton. In order to identify the flavor of the other (''tag'') B meson, we restrict the analysis to events in which another charged lepton (the ''tagging lepton'') is found. To reduce contamination from fake leptons and leptons originating from charm decays, we require that the momentum of this second lepton exceed 1.0 GeV/c for electrons, and 1.1 GeV/c for muons.

The decay point of the tag B is determined with the high-momentum lepton and a beam-spot constraint; the procedure is the same as that used to determine the $\overline{B}^0$ vertex. We compute Δt from the projected distance between the two vertices along the beam direction (z axis), $\Delta z = z_{\rm decay} - z_{\rm tag}$, with the approximation that the B^0 and the $\overline{B}^0$ are at rest in the $\Upsilon(4S)$ rest frame (the boost approximation): $\Delta t = \Delta z / c\beta\gamma$, where the boost factor $\beta\gamma$ is determined from the measured beam energies. To remove badly reconstructed vertices we reject all events with either $|\Delta z| > 3$ mm or $\sigma(\Delta z) > 0.5$ mm, where $\sigma(\Delta z)$ is the uncertainty on Δz, computed for each event. The simulation shows that the difference between the true and measured Δt can be fitted with the sum of two Gaussians. The rms of the narrow Gaussian, which describes 70% of the events, is 0.64 ps; the rms of the wide one is about 1.7 ps.

We then select the best right-charge candidate in each event according to the following procedure: if there is more than one, we choose that with $\mathcal{M}_\nu^2 > -2.5$ GeV$^2/c^4$. If two or more candidates are still left, but they have different leptons, we select the one with the largest value of χ. In a small fraction of events we select two or more candidates sharing the same lepton combined with different soft pions. We keep the candidate with the largest χ, unless one of the π_s^+ is consistent with coming from the decay of a D^{*+} from the other B, in which case we remove the event. For this purpose, we define the square of the missing neutrino mass in the tag-side, $\mathcal{M}^2_{\nu,tag-B}$, by means of Eq. (2), where we replace the four-momentum of the lepton from the $\overline{B}^0 \to D^{*+}\ell^-\bar{\nu}_\ell$ decay with that of the tag lepton. This variable peaks at zero for soft pions originating from the tag-B decay. We require $\mathcal{M}^2_{\nu,tag-B} < -3$ GeV$^2/c^4$. Finally we reject the events in which the signal lepton can be combined to a wrong-charge pion to produce an otherwise successful candidate, if the pion is consistent with coming from a D^{*+} from the tag-B according to the criterion just described. About 20% of the signal events are removed by this requirement.

For background studies, we select events in the region $\mathcal{M}_\nu^2 < -2.5$ GeV$^2/c^4$ if there is no candidate in the signal region. We find about 49 000 signal events over a background of about 28 000 events in the data sample in the region $\mathcal{M}_\nu^2 > -2.5$ GeV$^2/c^4$.

C. Sample composition

Our data sample consists of the following event types, categorized according to their origin and to whether or not they peak in the $\mathcal{M}_\nu^2$ distribution. We consider signal to be any combination of a lepton and a charged D^* produced in the decay of a single $\overline{B}^0$ meson. Signal consists of mainly $\overline{B}^0 \to D^{*+}\ell^-\bar{\nu}_\ell$ decays, with minor contributions from $\overline{B}^0 \to D^{*+}\pi^0\ell^-\overline{\nu}_\ell$, $\overline{B}^0 \to D^{*+}\tau^-\overline{\nu}_\tau$, $\overline{B}^0 \to D^{*+}D_s^-$, and $\overline{B}^0 \to D^{*+}\overline{D}X$ with τ, D_s^-, or $\overline{D}$ decaying to an ℓ^-, and from $\overline{B}^0 \to D^{*+}h$, with the hadron h misidentified as a muon. Peaking B^- background is mainly due to the processes $B^- \to D^{*+}\pi^-\ell^-\overline{\nu}_\ell$, and $B^- \to D^{*+}\pi^- X$ with the π^- misidentified as a muon. Other minor contributions to the peaking sample are due to decays $B \to D^*\pi\nu_\tau\tau$ ($\tau \to \ell X$), $B \to D^*\pi\overline{D}X$ ($\overline{D} \to \ell Y$), where the D^* and the π come from the decay of an orbitally excited D meson (D^{**}). Nonpeaking contributions are due to random combinations of a charged lepton candidate and a low-momentum pion candidate, produced either in $B\overline{B}$ events ($B\overline{B}$ combinatorial) or in $e^+e^- \to q\overline{q}$ interactions with $q = u, d, s$, or c (continuum). We compute the sample composition separately for mixed and unmixed events by fitting the corresponding $\mathcal{M}_\nu^2$ distribution to the sum of four components: continuum, $B\overline{B}$ combinatorial background, $\overline{B}^0 \to D^{*+}\ell^-\bar{\nu}_\ell$ decays, and $B \to D^*\pi\ell^-\bar{\nu}_\ell$ decays. Because of one or more additional pions in the final state, the $B \to D^*\pi\ell^-\bar{\nu}_\ell$ events have a different $\mathcal{M}_\nu^2$ spectrum from that of the process $\overline{B}^0 \to D^{*+}\ell^-\bar{\nu}_\ell$. We measure the continuum contribution from the off-resonance sample, scaled to the luminosity of the on-resonance sample. We determine the $\mathcal{M}_\nu^2$ distributions for the other event types from the simulation, and determine their relative abundance in the selected sample from a fit to the $\mathcal{M}_\nu^2$ distribution for the data. Assuming isospin conservation, we assign two-thirds of $B \to D^*\pi\ell^-\bar{\nu}_\ell$ decays to peaking B^- background and the rest to $\overline{B}^0 \to D^*\pi\ell^-\overline{\nu}_\ell$, which we add to the signal. We vary this fraction in the study of systematic uncertainties. We assume 50% uncertainty on the isospin-conservation hypothesis.

A possible distortion in the $\mathcal{M}_\nu^2$ distribution comes from the decay chain $\overline{B} \to D(X)\ell^-\overline{\nu}_\ell$, $D \to Y\pi^+$, where the state Y is so heavy that the charged pion is emitted at low momentum, behaving like a π_s^+ . This possibility has been extensively studied by the CLEO Collaboration [13], where the three D^+ decay modes most likely to cause this distortion have been identified: $\overline{K}^{*0}\omega\pi^+$, $K^{*-}\rho^+\pi^+$, and $\overline{K}^{*0}\rho^0\pi^+$. If we remove these events from the simulated

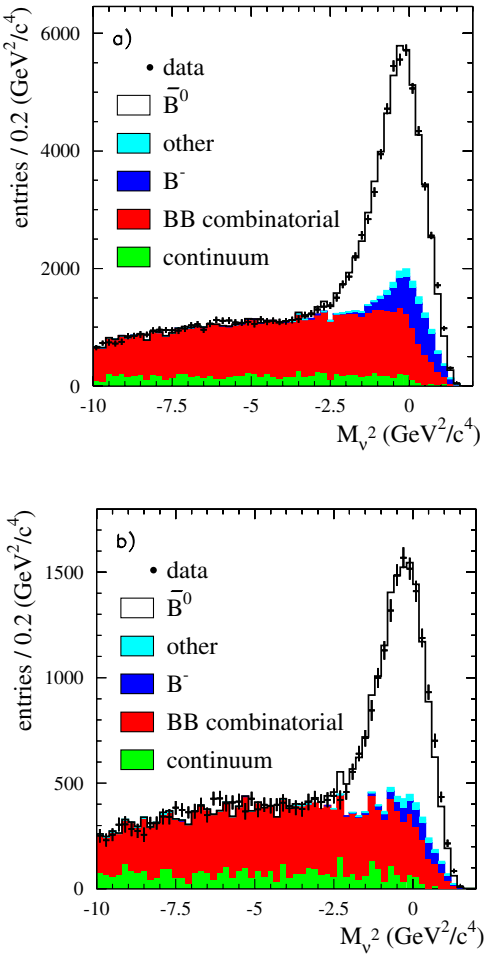

FIG. 3 (color online). Fit to the $\mathcal{M}_\nu^2$ distribution for the unmixed events (a) and mixed events (b). "$\overline{B}^0$" includes $\overline{B}^0 \to D^{*+}\ell^-\bar{\nu}_\ell$, $\overline{B}^0 \to D^{*+}\pi^0\ell^-\bar{\nu}_\ell$, $\overline{B}^0 \to D^{*+}\tau^-\bar{\nu}_\tau$ ($\tau \to \ell X$), $\overline{B}^0 \to D^{*+}D_s^-$ ($D_s \to \ell X$), $\overline{B}^0 \to D^{*+}\overline{D}X$ ($\overline{D} \to \ell Y$), and $\overline{B}^0 \to D^{*+}h$ with the hadron h misidentified as a muon. "B^-" includes $B^- \to D^{*+}\pi^-\ell^-\bar{\nu}_\ell$ and $B^- \to D^{*+}\pi^-X$ with the π^- misidentified as a muon. "Other" includes $B \to D^*\pi\nu_\tau\tau$ ($\tau \to \ell X$), $B \to D^*\pi\overline{D}X$ ($\overline{D} \to \ell Y$).

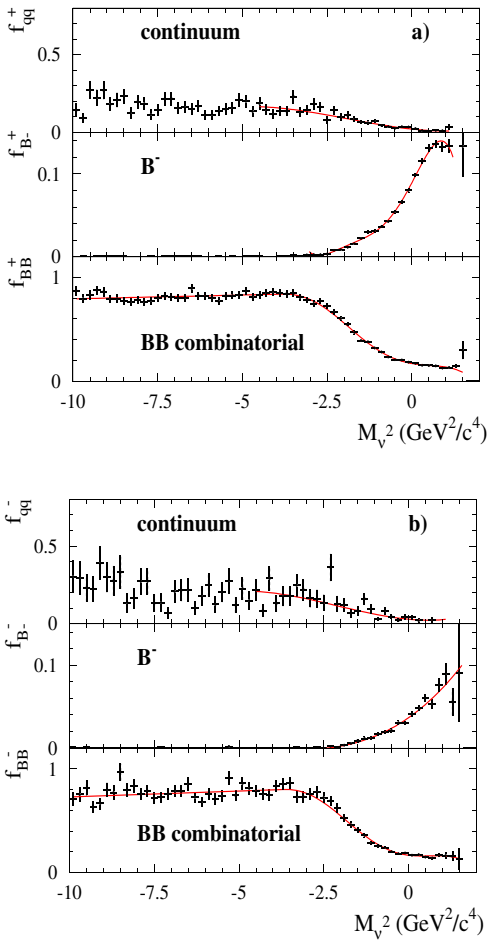

FIG. 4 (color online). Fraction of continuum events, peaking B^-, and $B\overline{B}$ combinatorial background in the unmixed (a) and mixed (b) lepton-tagged samples. The continuous lines overlaid represent the analytic functions ($f_{qq}^\pm$, $f_{B^-}^\pm$ and $f_{B\overline{B}}^\pm$) used to parametrize the distributions. The fraction of continuum events is parametrized only in the region $\mathcal{M}_\nu^2 > -4.5$ GeV$^2/c^4$. For $\mathcal{M}_\nu^2 < -4.5$ GeV$^2/c^4$, where just continuum and combinatorial backgrounds are present, we assume that $f_{B^-}^\pm = 0$, and we compute $f_{qq}^\pm = 1 - f_{B\overline{B}}^\pm$.

sample, and we repeat the fit, the number of fitted signal events increases by 0.4%. We assume therefore $\pm 0.4\%$ systematic error on the fraction of signal events in the sample due to this uncertainty.

Figure 3 shows the $\mathcal{M}_\nu{}^2$ fit results for unmixed (upper) and mixed (lower) events. We use the results of this study to determine the fraction of continuum ($f_{qq}^\pm$), $B\overline{B}$ combinatorial ($f_{B\overline{B}}^\pm$), and peaking B^- ($f_{B^-}^\pm$) background as a function of $\mathcal{M}_\nu^2$, separately for mixed (f^-) and unmixed (f^+) events. We parametrize these fractions with polynomial functions of $\mathcal{M}_\nu^2$ as shown in Fig. 4.

D. τ_{B^0} and Δm_d determination

We fit data and Monte Carlo events with a binned maximum-likelihood method. We divide the events into 100 Δt bins, spanning the range -18 ps $< \Delta t < 18$ ps, and 20 $\sigma_{\Delta t}$ bins between 0 and 3 ps. We assign to all events in each bin the values of Δt and $\sigma_{\Delta t}$ corresponding to the center of the bin. We fit simultaneously the mixed and unmixed events. We maximize the likelihood

$$\mathcal{L} = \left(\prod_{k=1}^{\mathcal{N}_{\rm unmix}} \mathcal{F}_k^+\right)\left(\prod_{j=1}^{\mathcal{N}_{\rm mix}} \mathcal{F}_j^-\right) \times C_{S_{B^-}} \times C_{\chi_d}, \quad (3)$$

where the indices k and j denote the unmixed and mixed selected events. The functions $\mathcal{F}^\pm(\Delta t, \sigma_{\Delta t}, \mathcal{M}_\nu^2 | \tau_{B^0}, \Delta m_d)$ describe the normalized Δt distribution as the sum of the decay probabilities for signal and background events:

$$\mathcal{F}^{\pm}(\Delta t, \sigma_{\Delta t}, \mathcal{M}_\nu^2|\tau_{B^0}, \Delta m_d) = f^{\pm}_{q\bar{q}}(\mathcal{M}_\nu^2)\cdot\mathcal{F}^{\pm}_{q\bar{q}}(\Delta t, \sigma_{\Delta t}) + f^{\pm}_{B\overline{B}}(\mathcal{M}_\nu^2)\cdot\mathcal{F}^{\pm}_{B\overline{B}}(\Delta t, \sigma_{\Delta t}) + S_{B^-}f^{\pm}_{B^-}(\mathcal{M}_\nu^2)\cdot\mathcal{F}^{\pm}_{B^-}(\Delta t, \sigma_{\Delta t}) + [1 - S_{B^-}f^{\pm}_{B^-}(\mathcal{M}_\nu^2) - f^{\pm}_{B\overline{B}}(\mathcal{M}_\nu^2) - f^{\pm}_{q\bar{q}}(\mathcal{M}_\nu^2)]\cdot\mathcal{F}^{\pm}_{\overline{B}^0}(\Delta t, \sigma_{\Delta t}|\tau_{B^0}, \Delta m_d), \quad (4)$$

where the functions $\mathcal{F}_i^{\pm}$ represent the probability density functions (PDF) for signal ($i = \overline{B}^0$), peaking B^- ($i = B^-$), $B\overline{B}$ combinatorial ($i = B\overline{B}$), and continuum ($i = q\overline{q}$) events, modified to account for the finite resolution of the detector, and the superscript $+(-)$ applies to unmixed (mixed) events. The resolution function is expressed as the sum of three Gaussian functions, described as ''narrow,'' ''wide,'' and ''outlier'':

$$\mathcal{R}(\delta\Delta t, \sigma_{\Delta t}) = \frac{(1 - f_w - f_o)}{\sqrt{2\pi}S_n\sigma_{\Delta t}}e^{-(\delta\Delta t - o_n)^2/2S_n^2\sigma_{\Delta t}^2} + \frac{f_w}{\sqrt{2\pi}S_w\sigma_{\Delta t}}e^{-(\delta\Delta t - o_w)^2/2S_w^2\sigma_{\Delta t}^2} + \frac{f_o}{\sqrt{2\pi}S_o}e^{-(\delta\Delta t - o_o)^2/2S_o^2},$$

where $\delta\Delta t$ is the difference between the measured and true values of Δt, o_n and o_w are offsets, and the factors S_n and S_w account for possible misestimation of $\sigma_{\Delta t}$. The outlier term, described by a Gaussian function of fixed width S_o and offset o_o, is introduced to describe events with badly measured Δt, and accounts for less than 1% of the events.

To account for the $\pm 50\%$ uncertainty on the isospin assumption (see Sec. III C), the functions $f^+_{B^-}$ and $f^-_{B^-}$ are multiplied in the PDF for the peaking B^- background by a common scale factor S_{B^-}. This parameter is allowed to vary in the fit, constrained to unity with variance $\sigma_{B^-} = 0.5$ by means of the Gaussian term

$$C_{S_{B^-}} = e^{-(S_{B^-}-1)^2/2\sigma^2_{B^-}}.$$

We constrain the expected fraction $P_{\rm exp}$ of mixed events to the observed one

$$P_{\rm obs} = \frac{\mathcal{N}_{\rm mix}}{\mathcal{N}_{\rm mix} + \mathcal{N}_{\rm unmix}}$$

by means of the binomial factor

$$C_{\chi_d} = \frac{\mathcal{N}!}{\mathcal{N}_{\rm mix}!\mathcal{N}_{\rm unmix}!}P_{\rm exp}^{\mathcal{N}_{\rm mix}}(1 - P_{\rm exp})^{\mathcal{N}_{\rm unmix}}.$$

For a sample of signal events with dilution $\mathcal{D}$, the expected fraction reads

$$P_{\rm exp}(\Delta m_d, \tau_{B^0}, \mathcal{D}) = \chi_d\cdot\mathcal{D} + \frac{1 - \mathcal{D}}{2},$$

where, neglecting the decay-rate difference $\Delta\Gamma_d$ between the two mass eigenstates, the integrated mixing rate χ_d is related to the product $x = \Delta m_d\cdot\tau_{B^0}$ by the relation

$$\chi_d = \frac{x^2}{2(1 + x^2)}.$$

We divide signal events according to the origin of the tag lepton into primary ($\mathcal{P}\ell$), cascade ($C\ell$), and decay-side ($\mathcal{D}\ell$) lepton tags. A primary lepton tag is produced in the direct decay $B^0 \to \ell^+\nu_\ell X$. These events are described by Eq. (1), with $\mathcal{D}$ close to 1 (a small deviation from unity is expected due to hadron misidentification, leptons from J/ψ, etc.). We expect small values of o_n and o_w for primary tags, because the lepton originates from the B^0 decay point.

Cascade lepton tags, produced in the process $B^0 \to DX, D \to \ell Y$, are suppressed by the requirement on the lepton momentum but still exist at a level of 9%, which we determine by varying their relative abundance ($f_{C\ell}$) as an additional parameter in the Δm_d and τ_{B^0} fit on data. The cascade lepton production point is displaced from the B^0 decay point due to the finite lifetime of charm mesons and the e^+e^- energy asymmetry. This results in a significant negative value of the offsets for this category. Compared with the primary lepton tag, the cascade lepton is more likely to have the opposite charge correlation with the B^0 flavor. The same charge correlation is obtained when the charm meson is produced from the hadronization of the virtual W from B^0 decay, which can result in the production of two opposite-flavor charm mesons. We account for these facts by applying Eq. (1) to the cascade tag events with negative dilution $\mathcal{D}_{C\ell} = -(1 - 2f^{\bar{b}\to c\to\ell^+}_{C\ell}) = -0.65 \pm 0.08$, where we take from the PDG [14] the ratio

$$f^{\bar{b}\to c\to\ell^+}_{C\ell} = \frac{\mathcal{B}(\bar{b}\to c\to\ell^+)}{\mathcal{B}(\bar{b}\to c\to\ell^+) + \mathcal{B}(\bar{b}\to\bar{c}\to\ell^-)} = 0.17 \pm 0.04.$$

The contribution to the dilution from other sources associated with the $\pi_s^+\ell^-$ candidate, such as fake hadrons, is negligible.

Decay-side tags are produced by the semileptonic decay of the unreconstructed D^0. Therefore they do not carry any information about τ_{B^0} or Δm_d. The PDF for both mixed and unmixed contributions is a purely exponential function, with an effective lifetime τ_{D_e} representing the displacement of the lepton production point from the $\overline{B}^0$ decay point due to the finite lifetime of the D^0. We determine the fraction of these events by fitting the $\cos\theta_{\pi_s^+\ell^-}$ distribution [see plots in Figs. 5(a) and 6(a)], where $\theta_{\pi_s^+\ell^-}$ is the angle between the soft pion and the tag lepton in the e^+e^- rest frame. We fit the data with the sum of the histograms for signal events, $B\overline{B}$ combinatorial background, and peaking B^- background obtained from the simulation, and continuum background obtained from the off-resonance events. We fix the fraction of signal events, peaking B^- background, $B\overline{B}$ combinatorial background and continuum

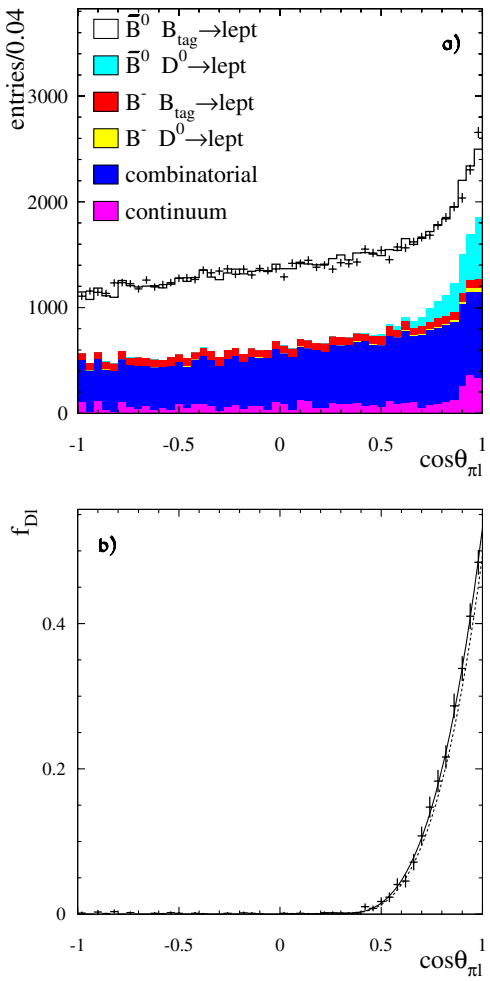

FIG. 5 (color online). Distribution of $\cos\theta_{\pi_s^+\ell^-}$ for unmixed events. In (a), the points with error bars represent the data, and the histograms show the various sample components determined by the fit; (b) shows the ratio between the fraction of tags from D^0 decays over the total number of tags in signal events, as obtained from the simulation rescaled to the result of the fit. This distribution is parametrized by a third-order polynomial represented by the continuous line overlaid. The dotted line represents the corresponding distribution obtained without rescaling the simulation to the fit result.

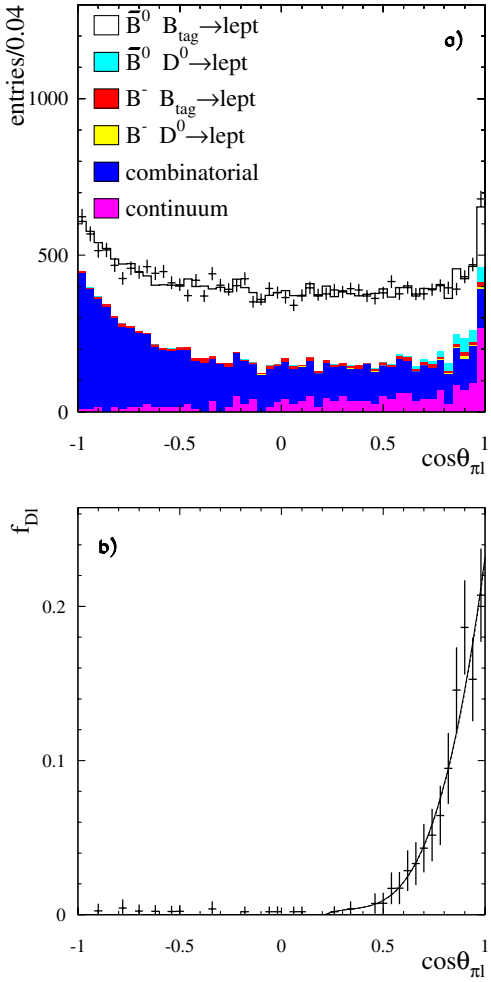

FIG. 6 (color online). Same as Fig. 5 for mixed events.

background in the fit and we allow to vary the relative amount of decay-side tags and tag-side tags.

Using the results of the $\cos\theta_{\pi_s^+\ell^-}$ fit we parametrize the probability for each event to have a decay-side tag as a third-order polynomial function of $\cos\theta_{\pi_s^+\ell^-}$ [see plots in Figs. 5(b) and 6(b)].

The signal PDF for both mixed and unmixed events consists of the sum of PDFs for primary, cascade, and decay-side tags, each convoluted with its own resolution function. The parameters S_n, S_w, S_o, f_w, and f_o are common to the three terms, but each tag type has different offsets (o_n, o_w). All the parameters of the resolution functions, the dilution of the primary tags, the fraction of cascade tags, and the effective lifetime of the decay-side tags are free parameters in the fit. We fix the other parameters (dilution of cascade tags, fraction of decay-side tags) to the values obtained as described above, and then vary them within their uncertainties to assess the corresponding systematic error.

We adopt a similar PDF for peaking B^- background, with separate primary, cascade, and decay-side terms. Because B^- mesons do not oscillate, we use a pure exponential PDF for the primary and cascade tags with lifetime $\tau_{B^-} = 1.671$ ps [15]. We force the parameters of the resolution function to equal those for the corresponding signal term.

We describe continuum events with an exponential function convoluted with a three-Gaussian resolution function. The mixed and unmixed terms have a common effective lifetime τ_{lq}. All the parameters of the continuum resolution function are set equal to those of the signal, except for the offsets, which are free in the fit.

The PDF for combinatorial $B\overline{B}$ background accounts for oscillating and nonoscillating subsamples. It has the same functional form as the PDF for peaking events, but with

independent parameters for the oscillation frequency, the lifetimes and the fractions of B^- background, primary, cascade, and decay-side tag events. The parameters S_w, f_w and o_o are set to the same values as those in the signal PDF.

IV. RESULTS

We first apply the measurement procedure on several Monte Carlo samples. We validate each term of the PDF by first fitting signal events, for primary, cascade and decay-side tags separately, and then adding them together. We then add peaking B^- background, and finally add the $B\overline{B}$ combinatorial background. We observe the following features:

(i) The event selection introduces no bias on τ_{B^0} and a bias of (-0.0029 ± 0.0010) ps^{-1} on Δm_d.

(ii) The boost approximation introduces a bias on τ_{B^0} (+ 0.0054 ps) and an additional bias on Δm_d (− 0.0034 ps^{-1}), determined by fitting the true Δz distribution. These biases disappear however when we fit the smeared Δz and allow for the experimental resolution in the fit function.

(iii) After the introduction of B^- peaking background we observe a bias of (-0.0079 ± 0.0064) ps on τ_{B^0} and (-0.0034 ± 0.0028) ps^{-1} on Δm_d.

(iv) Adding combinatorial $B\overline{B}$ events, we observe a bias of $(+0.0063 \pm 0.0070)$ ps on τ_{B^0} and (-0.0074 ± 0.0035) ps^{-1} on Δm_d.

(v) The isospin scale factor $S_{B^-} = 0.91 \pm 0.10$ is consistent with unity.

Based on these observations, we correct the data results by subtracting 0.0063 ps from τ_{B^0}, and adding 0.0074 ps^{-1} to Δm_d. We include the Monte Carlo statistical errors of ± 0.0070 ps for τ_{B^0} and ± 0.0035 ps^{-1} for Δm_d as systematic uncertainties.

We determine the parameters for continuum events directly from the fit to on-resonance data, and we independently fit the off-resonance events to verify the consistency with the on-resonance continuum results.

TABLE I. Parameters used in the PDFs. The upper set of parameters refers to peaking events; the lower one refers to those parameters of the resolution function that are common to all the event types. The second column shows how the parameters are treated in the fit. The third (fourth) column gives the result of the fit on data (MC) for free parameters and the value employed for the parameters that are fixed or used as a constraint. The quoted error is the statistical uncertainty from the fit for free parameters and the range of variation used in the systematic error determination for the others. The last column shows the sample in which the parameter is used. $\mathcal{P}\ell$, $C\ell$ and $\mathcal{D}\ell$ refer to primary, cascade and decay-side lepton tags, respectively. The parameters o, S, and f correspond to offsets, scale factors, and fractions in the resolution function.

Parameter	Usage	Data	MC	Sample
τ_{B^0} (ps)	Free	1.510 ± 0.013	1.554 ± 0.007	$\overline{B}^0$ $P\ell$, $C\ell$
Δm_d (ps^{-1})	Free	0.503 ± 0.007	0.465 ± 0.004	$\overline{B}^0$ $P\ell$, $C\ell$
τ_{D_e}(ps)	Free	0.12 ± 0.04	0.21 ± 0.02	$\overline{B}^0$, B^-, $B\overline{B}$ $D\ell$
τ_{B^-} (ps)	Fixed	1.671 ± 0.018	1.65	B^-, $B\overline{B}$
S_{B^-}	Constr. (1.0 ± 0.5)	1.05 ± 0.15	0.91 ± 0.10	
$f_{C\ell}$	Free	0.095 ± 0.006	0.066 ± 0.004	$\overline{B}^0$
$D_{\mathcal{P}\ell}$	Free	1.00 ± 0.02	0.970 ± 0.006	$\overline{B}^0$, $P\ell$
$D_{C\ell}$	Fixed	-0.65 ± 0.08	-0.545	$\overline{B}^0$, $C\ell$
$o_{\mathcal{P}\ell,n}$ $(= o_{\mathcal{P}\ell,w})$	Free	-0.019 ± 0.011	-0.012 ± 0.007	$\overline{B}^0$, B^- $P\ell$
$o_{C\ell,n}$	Free	-0.18 ± 0.07	-0.43 ± 0.07	$\overline{B}^0$ $C\ell$
$o_{C\ell,w}$	Free	2.8 ± 1.1	-5.8 ± 0.7	$\overline{B}^0$ $C\ell$
$o_{\mathcal{D}\ell,n}$ $(= o_{\mathcal{D}\ell,w})$	Free	-0.12 ± 0.03	-0.14 ± 0.02	$\overline{B}^0$, B^-, $D\ell$
S_n	Free	0.952 ± 0.015	1.007 ± 0.006	All
S_o (ps)	Free	12.8 ± 5.6	17.9 ± 8.2	$\overline{B}^0$, B^-
f_o	Free	0.0013 ± 0.0005	0.0008 ± 0.0003	$\overline{B}^0$, B^-
S_w	Free	2.57 ± 0.13	2.63 ± 0.15	All
f_w	Free	0.050 ± 0.005	0.035 ± 0.005	All
o_o	Fixed	0	0	All

TABLE II. Parameters used in the background PDF. The upper set of parameters refers to $B\overline{B}$ combinatorial events, the central one refers to continuum parameters, and the lower set refers to those parameters of the resolution function that are common to all event types. The symbols α correspond to the fractions of decay-side tags in the different samples. The last line shows the statistical correlation between τ_{B^0} and Δm_d.

Parameter	Usage	Data	M.C.	Sample
$\tau_{B^0}^{BKG}$ (ps)	Free	1.22 ± 0.07	1.37 ± 0.07	$B\overline{B}$
Δm_d^{BKG} (ps^{-1})	Free	0.37 ± 0.06	0.42 ± 0.04	$B\overline{B}$
$\tau_{B^-}^{BKG}$ (ps)	Fixed	1.671 ± 0.018	1.65	B^-, $B\overline{B}$
$f_{C\ell,u}^{BKG}$	Fixed	0.030 ± 0.006	0.030	$B\overline{B}$ ($\overline{B}^0$ only)
$f_{C\ell,m}^{BKG}$	Free	0.041 ± 0.022	0.069 ± 0.021	$B\overline{B}$ ($\overline{B}^0$ only)
$f_{B-,u}^{BKG}$	Free	0.62 ± 0.08	0.52 ± 0.02	$B\overline{B}$
$f_{B-,m}^{BKG}$	Free	0.15 ± 0.10	0.11 ± 0.04	$B\overline{B}$
$\alpha_{B0,u}^{BKG}$	Free	0.11 ± 0.19	0.25 ± 0.03	$B\overline{B}$ ($\overline{B}^0$ only)
$\alpha_{B0,m}^{BKG}$	Fixed	0.065 ± 0.013	0.065	$B\overline{B}$ ($\overline{B}^0$ only)
$\alpha_{B-,u}^{BKG}$	Free	0.21 ± 0.10	0.20 ± 0.02	$B\overline{B}$ ($\overline{B}^-$ only)
$\alpha_{B-,m}^{BKG}$	Fixed	0.36 ± 0.07	0.36	$B\overline{B}$ (B^- only)
$f_{\mathcal{D}\ell,2}$	Fixed	0.60 ± 0.12	0.60 ± 0.12	$B\overline{B}$, $D\ell$
$D_{\mathcal{P}\ell}^{BKG}$	Free	0.989 ± 0.013	0.964 ± 0.006	$B\overline{B}$ ($\overline{B}^0$ only)
$D_{C\ell}^{BKG}$	Fixed	-0.65 ± 0.08	-0.545	$B\overline{B}$ ($\overline{B}^0$ only)
$o_{\mathcal{P}\ell}^{BKG}$	Free	-0.006 ± 0.016	-0.02 ± 0.03	$B\overline{B}$, $P\ell$
$o_{C\ell}^{BKG}$	Free	-1.6 ± 0.6	-0.8 ± 0.2	$B\overline{B}$, $C\ell$
$o_{\mathcal{D}\ell}^{BKG}$	Free	-0.02 ± 0.04	-0.05 ± 0.03	$B\overline{B}$, $D\ell$
S_n^{BKG}	Free	0.961 ± 0.015	0.961 ± 0.021	All
S_o^{BKG} (ps)	Free	10.4 ± 3.6	14.7 ± 6.1	$B\overline{B}$
f_o^{BKG}	Free	0.0021 ± 0.0009	0.0008 ± 0.0003	$B\overline{B}$
τ_{lq} (ps)	Free	0.27 ± 0.05	-	Continuum
$o_{lq,n}$ $(= o_{lq,w})$	Free	0.007 ± 0.032	-	Continuum
S_w	Free	2.57 ± 0.13	2.63 ± 0.15	All
f_w	Free	0.050 ± 0.005	0.035 ± 0.005	All
o_o	Fixed	0	0	All
$\rho(\tau_{B^0}, \Delta m_d)$		0.007	-0.127	

We finally perform the fit to the on-resonance data. Together with Δm_d and τ_{B^0}, we allow to vary most of the parameters describing the peaking B^-, $B\overline{B}$ combinatorial, and continuum background events. The results of the fits to the Monte Carlo and data samples are shown in Tables I and II.

The fit results are $\tau_{B^0} = (1.510 \pm 0.013(\mathrm{stat}))$ ps, and $\Delta m_d = (0.5035 \pm 0.0068(\mathrm{stat}))\ \mathrm{ps}^{-1}$. We correct these values for the biases measured in the Monte Carlo simulation, obtaining the results

$$\tau_{B^0} = (1.504 \pm 0.013(\mathrm{stat}))\ \mathrm{ps},$$
$$\Delta m_d = (0.5109 \pm 0.0068(\mathrm{stat}))\ \mathrm{ps}^{-1}.$$

The statistical correlation between Δm_d and τ_{B^0} is 0.7%. Δm_d has sizable correlations with S_{B^-} (50%) and with the fraction of cascade tags (24%). τ_{B^0} is correlated with S_n (-27%) and the offset of the wide Gaussian for the cascade tags (-31%). The complete set of fit parameters is reported in Tables I and II.

Details on the systematic error are reported in Sec. V. Figures 7 and 8 show the comparison between the data and the fit function projected on Δt, for a sample of events enriched in signal by the cut $\mathcal{M}_\nu^2 > -2.5\ \mathrm{GeV}^2/c^4$; Figs. 9 and 10 show the same comparison for events in the background region.

Figures 11 and 12 show plots of the time-dependent asymmetry

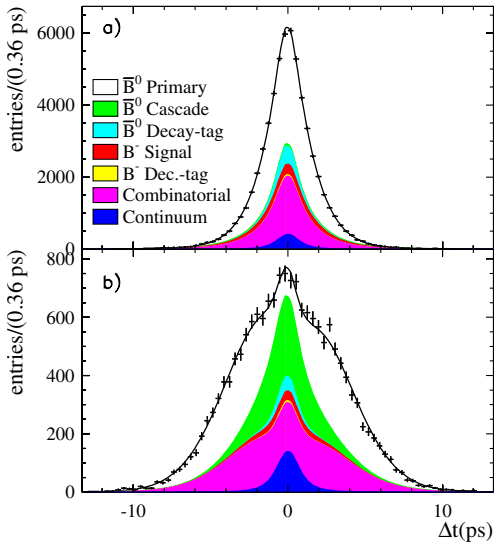

FIG. 7 (color online). Distribution of Δt for unmixed (a) and mixed (b) events in the signal $\mathcal{M}_\nu^2$ region. The points show the data, the curve is the projection of the fit result, and the shaded areas from bottom to top are the contributions from continuum background, $B\overline{B}$ combinatorial background, peaking B^- background with decay-side tag, peaking B^- background with primary tag, signal with decay-side tag, signal with cascade tag, and signal with primary tag.

$$\mathcal{A}(\Delta t) = \frac{\mathcal{N}_{\rm unmix}(\Delta t) - \mathcal{N}_{\rm mix}(\Delta t)}{\mathcal{N}_{\rm unmix}(\Delta t) + \mathcal{N}_{\rm mix}(\Delta t)}$$

for events in the $\mathcal{M}_\nu^2$ signal region and events in the $\mathcal{M}_\nu^2$ background region. For signal events, neglecting Δt resolution, $\mathcal{A}(\Delta t) = \mathcal{D}\cos(\Delta m_d \Delta t)$ [see Eq. (1)].

The agreement between the fit function and the data distribution is good in both the signal and background regions. The asymmetry is quite significant for events in the background $\mathcal{M}_\nu^2$ region because a large fraction of these events are due to combinatorial $B^0\overline{B}^0$ background.

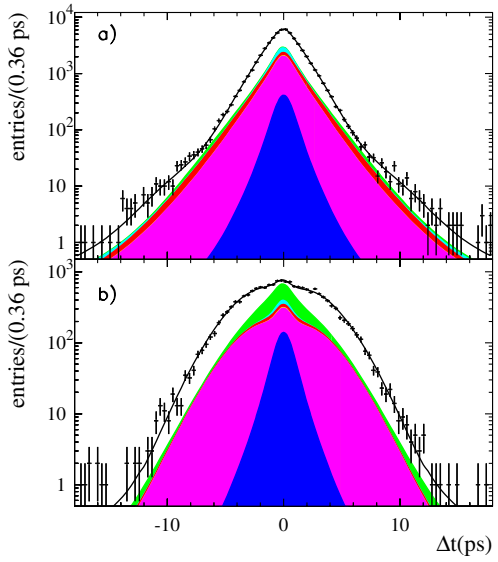

FIG. 8 (color online). Same as Fig. 7 with logarithmic scale.

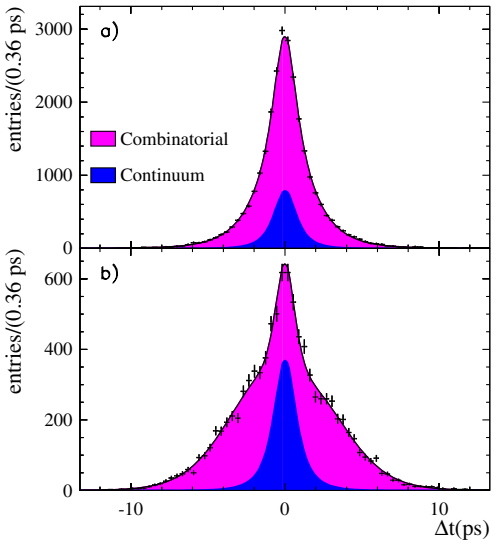

FIG. 9 (color online). Distribution of Δt for unmixed (a) and mixed (b) events in the background $\mathcal{M}_\nu^2$ region. The points show the data, the curve is the projection of the fit result, and the shaded areas are the contributions from continuum and $B\overline{B}$ combinatorial background.

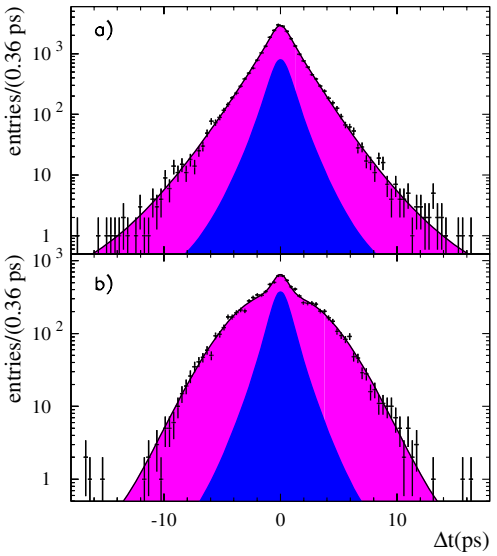

FIG. 10 (color online). Same as Fig. 9 with logarithmic scale.

V. SYSTEMATIC UNCERTAINTIES

The systematic errors are summarized in Table III. We consider the following sources of systematic uncertainty:

(1) *Sample composition.*—We calculate a total uncertainty of $\pm 1.3\%$ on the number of signal events. This uncertainty is the quadratic sum of the statistical error in the $\mathcal{M}_\nu^2$ fit ($\pm 1.2\%$), the systematic uncertainty on the shape of $B\overline{B}$ combinatoric back-

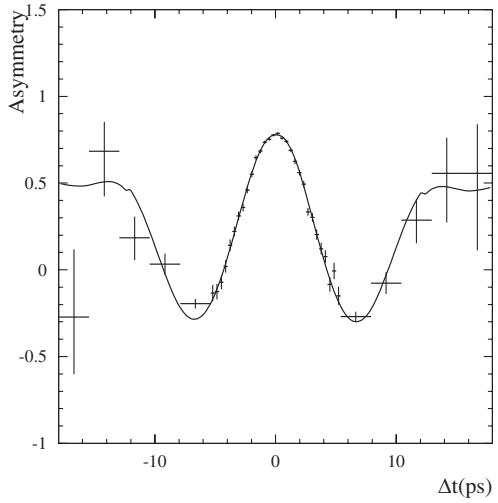

FIG. 11. Asymmetry between unmixed and mixed events as a function of Δt, for events in the signal $\mathcal{M}_\nu^2$ region. Points with error bars represent the data, and the curve is a projection of the fit result.

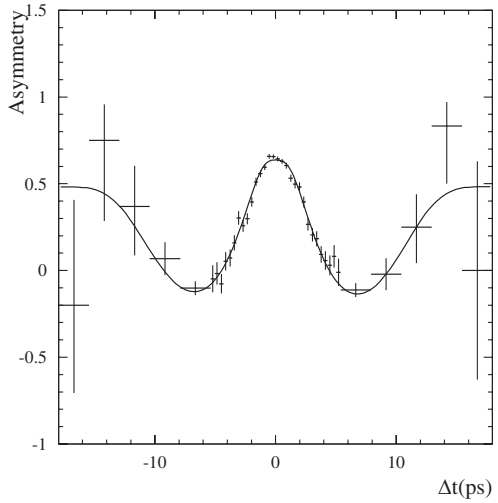

FIG. 12. Asymmetry between unmixed and mixed events as a function of Δt, for events in the background $\mathcal{M}_\nu^2$ region. Points with error bars represent the data, and the curve is a projection of the fit result.

ground from the test on the ''wrong-charge'' sample ($\pm$ 0.2%) (see Sec. III A), and the additional systematic uncertainty due to low-momentum pions from D^+ decays ($\pm$ 0.4%) (see Sec. III C).

(2) *Analysis bias (entry b).*—We use the statistical error on the bias observed in the fit on the Monte Carlo sample.

(3) *Signal and background PDF description.*—Most of the parameters in the PDF are free in the fit and therefore do not contribute to the systematic error. We vary the parameters that are fixed in the fit by their uncertainty, repeat the fit, and use the corresponding variation in τ_{B^0} and Δm_d as systematic errors. We take the uncertainty on τ_{B^-} (entry c), and on $D_{C\ell}$ (entry d) from the PDG [14]. We find that four parameters used in the description of the combinatorial background, as determined by the fit on the Monte Carlo sample, are not in agreement with the Monte Carlo truth. They are the fraction of cascade tag-side leptons in the unmixed event sample, $f_{C\ell,u}^{BKG}$, the fraction of decay-side tags in the mixed $\overline{B}^0$ and the B^- event samples, $\alpha_{B0,m}^{BKG}$ and $\alpha_{B-,m}^{BKG}$, respectively, and an additional parameter used in the description of the shape of the proper time difference Δt of the decay-side tagged mixed sample, $f_{\mathcal{D}\ell,2}$. Therefore we fix them to the Monte Carlo prediction. We vary the value of each of them by 20% to compute the systematic error from the comparison with the default result, and we sum the four uncertainties in quadrature (entry e).

(4) *Detector alignment.*—We consider effects due to the detector z scale, determined by reconstructing protons scattered from the beam pipe and comparing the measured beam pipe dimensions with the optical survey data [16]. The z scale indetermination corresponds to an uncertainty of $\pm 0.4\%$ on Δt. We repeat the fit applying this scale correction to Δt, and use the variation with respect to the default result as the systematic error (entry f). From the measurement of the beam energies, the $\Upsilon(4S)$ Lorentz boost factor is determined with an uncertainty which translates into a $\pm 0.1\%$ indetermination on Δt. Again we repeat the fit and assume as systematic error the variation of the result (entry g). We then consider the effect of varying the beam-spot position by $\pm 40\mu$m in the y direction (entry h). We compute the uncertainty due to SVT time-dependent misalignment by comparing

TABLE III. Systematic uncertainties. See text for details.

Source	Variation	$\delta\tau_{B^0}$ (ps)	$\delta\Delta m_d$ (ps^{-1})
(a) Sample Composition	$\pm 1.3\%$	± 0.0003	∓ 0.0002
(b) Analysis bias		± 0.0070	∓ 0.0035
(c) τ_{B^-}	1.671 ± 0.018	∓ 0.0014	∓ 0.0008
(d) $\mathcal{D}_{C\ell}$	0.65 ± 0.08	∓ 0.0003	∓ 0.0003
(e) Combinatorial BKG		± 0.0007	∓ 0.0002
(f) z scale		± 0.0070	∓ 0.0020
(g) PEP-II boost		± 0.0020	∓ 0.0003
(h) Beam-spot position		± 0.0050	∓ 0.0010
(i) Alignment		$^{+0.0132}_{-0.0038}$	$^{-0.0038}_{+0.0033}$
(j) Decay-side tags		± 0.0013	
(k) Binning		∓ 0.0021	± 0.0006
(l) Outlier parameters		± 0.0028	± 0.0012
(m) Δt and $\sigma_{\Delta t}$ cut		± 0.0033	∓ 0.0033
(n) GExp model		-0.0016	$+0.0011$
Total		$^{+0.0182}_{-0.0131}$	$^{+0.0068}_{-0.0064}$

results obtained with different sets of alignment constants (entry i).

(5) *Decay-side tags.*—We vary the parameters describing the fraction of decay-side tags by their statistical errors, repeat the fit, and take the variation with respect to the default result as the systematic error (entry j).

(6) *Binned fitting*.—We vary the number of bins in Δt from 100 to 250 and in $\sigma_{\Delta t}$ from 20 to 50, and we repeat the fit. We take the systematic error to be the variation with respect to the default result (entry k).

(7) *Outlier description*.—We vary the value of the offset of the outlier Gaussian from -5 ps to $+5$ ps. As a cross-check, we use a PDF that is uniform in Δt for the description of the outliers. We take the maximum variation with respect to the default result as the systematic error (entry l).

(8) *Fit range*.—We vary the Δt fit range from ± 18 ps to ± 10 ps and the $\sigma_{\Delta t}$ maximum value from 1.8 to 4.2 ps. Again we assume the maximum variation between the various results and the default one as the systematic error (entry m).

(9) *Cascade lepton tag-side parametrization.*—For the resolution model, we use a Gaussian distribution convolved with a one-sided exponential to describe the core part of the resolution function (GExp) instead of the Gaussian resolution with a nonzero offset. We quote as systematic error the difference between the results obtained with the two different approaches (entry n).

VI. CONSISTENCY CHECKS

We rely on the assumption that the parameters of the background PDF do not depend on $\mathcal{M}_\nu^2$. We verify this assumption for the continuum background with the fit to the off-resonance events. To check this assumption for the $B\overline{B}$ combinatorial PDF, we perform several cross checks on the data and the Monte Carlo. We compare the simulated combinatorial $B\overline{B}$ Δt distribution in several independent regions of $\mathcal{M}_\nu^2$ with Kolmogorov-Smirnov tests and always obtain a reasonable probability for agreement. We fit the Δt distribution of combinatorial background $B\overline{B}$ events separately in the signal and background $\mathcal{M}_\nu^2$ region and compare the parameters of the PDF. We fit the signal plus $B\overline{B}$ background Monte Carlo events in the signal region only, fixing all the parameters of the $B\overline{B}$ background to the values obtained in a fit to the background region, and do not see any significant deviation from the results of the full fit. Finally, we repeat the fit on both the data and the Monte Carlo using different $\mathcal{M}_\nu^2$ ranges for the background region. Once again, we do not observe any significant difference in τ_{B^0} and Δm_d relative to the default result.

We repeat the analysis with a more stringent requirement on the combined signal likelihood (a minimum $\mathcal{X}$ of 0.5 rather than 0.4). No significant change in the result is observed.

We validate the fit procedure with a parametrized Monte Carlo simulation. We simulate several experiments from the fitted PDF of both the Monte Carlo and the data, with parameters fixed to the values obtained from the corresponding fit. Each experiment is produced with the same number of events as the original sample. For each experiment we produce seven data sets, corresponding to $\overline{B}^0$ with primary, cascade, and decay-side lepton tags, peaking B^- background with tag-side and decay-side lepton tags, $B\overline{B}$ combinatorial background, and continuum background. We fit every experiment with the same procedure as the corresponding original sample, and finally we compare the fitted parameters with the generated values. The result of this study is summarized in Table IV where we report the average and the root-mean-square deviation (rms) of the distribution of the difference between the fitted and the generated parameter value divided by the fit statistical error (pull). We do not find any significant statistical anomaly in the fit behavior.

We rely on the assumption that the decay-rate difference $\Delta\Gamma_d$ between the two mass eigenstates can be neglected in the analysis. We check this assumption with a parametrized Monte Carlo simulation in which events are simulated with zero mistag probability and perfect Δt resolution. We produce two sets of 100 Monte Carlo experiments. In the first set, $\Delta\Gamma_d = 0$; in the second, $\frac{\Delta\Gamma_d}{\Gamma_d} = 0.01$. We fit every experiment with the same procedure neglecting $\Delta\Gamma_d$ and we do not find any significant difference in the values of τ_{B^0} and Δm_d in the two different sets.

We investigate a possible analysis bias due to the finite τ and D_s lifetimes in $\overline{B}^0 \to D^{*+}\tau^-\bar{\nu}_\tau$ $(\tau^- \to \ell^- X)$ and $\overline{B}^0 \to D^{*+}D_s^-$ $(D_s^- \to \ell^- X)$ decays. We fit the Monte Carlo signal sample with no mistag and realistic Δt resolution after removing these decays and we do not find any significant variation with respect to the result obtained with the full signal sample.

TABLE IV. Results extracted from parametrized Monte Carlo experiments generated with parameters fixed to the values obtained from the fit to data (second column) and to the full Monte Carlo simulation (third column). For both τ_{B^0} and Δm_d the average and the rms of the distribution of the pull with respect to the generated value are reported.

Parameter	Data	Monte Carlo
Number of experiments	54	124
Pull τ_{B^0} average	0.38 ± 0.19	0.38 ± 0.12
Pull τ_{B^0} rms	1.13 ± 0.19	1.25 ± 0.13
Pull Δm_d average	-0.33 ± 0.17	0.08 ± 0.11
Pull Δm_d rms	1.14 ± 0.17	1.09 ± 0.08

VII. CONCLUSION

We have performed a measurement of Δm_d and τ_{B^0} with a sample of about 50 000 partially reconstructed, lepton-tagged $\overline{B}^0 \to D^{*+}\ell^-\bar{\nu}_\ell$ decays. We obtain the following results:

$$\tau_{B^0} = (1.504 \pm 0.013(\text{stat})^{+0.018}_{-0.013}(\text{syst}))\ \text{ps},$$

$$\Delta m_d = (0.511 \pm 0.007(\text{stat})^{+0.007}_{-0.006}(\text{syst}))\ \text{ps}^{-1}.$$

The τ_{B^0} value is consistent with the published measurement performed by *BABAR* using $\overline{B}^0 \to D^{*+}\ell^-\bar{\nu}_\ell$ partially reconstructed decays [5]. Our results are also consistent with published measurements of τ_{B^0} and Δm_d performed by *BABAR* with different data sets [6,17–20], and with the world averages computed by the Heavy Flavor Averaging Group for the PDG 2005 web update: $\tau_{B^0} = (1.532 \pm 0.009)$ ps, and $\Delta m_d = (0.505 \pm 0.005)\ \text{ps}^{-1}$.

ACKNOWLEDGMENTS

We are grateful for the extraordinary contributions of our PEP-II colleagues in achieving the excellent luminosity and machine conditions that have made this work possible. The success of this project also relies critically on the expertise and dedication of the computing organizations that support *BABAR*. The collaborating institutions wish to thank SLAC for its support and the kind hospitality extended to them. This work is supported by the U.S. Department of Energy and National Science Foundation, the Natural Sciences and Engineering Research Council (Canada), Institute of High Energy Physics (China), the Commissariat à l'Energie Atomique and Institut National de Physique Nucléaire et de Physique des Particules (France), the Bundesministerium für Bildung und Forschung and Deutsche Forschungsgemeinschaft (Germany), the Istituto Nazionale di Fisica Nucleare (Italy), the Foundation for Fundamental Research on Matter (The Netherlands), the Research Council of Norway, the Ministry of Science and Technology of the Russian Federation, and the Particle Physics and Astronomy Research Council (United Kingdom). Individuals have received support from CONACyT (Mexico), the A. P. Sloan Foundation, the Research Corporation, and the Alexander von Humboldt Foundation.

[1] N. Cabibbo, Phys. Rev. Lett. **10**, 531 (1963); M. Kobayashi and T. Maskawa, Prog. Theor. Phys. **49**, 652 (1973).
[2] Charge conjugate states are always implicitly assumed; ℓ means either electron or muon.
[3] B. Aubert *et al.* (*BABAR* Collaboration), Nucl. Instrum. Methods Phys. Res., Sect. A **479**, 1 (2002).
[4] G. C. Fox and S. Wolfram, Phys. Rev. Lett. **41**, 1581 (1978).
[5] B. Aubert *et al.* (*BABAR* Collaboration), Phys. Rev. Lett. **89**, 011802 (2002).
[6] B. Aubert *et al.* (*BABAR* Collaboration), Phys. Rev. D **67**, 091101 (2003).
[7] B. Aubert *et al.* (*BABAR* Collaboration), Phys. Rev. Lett. **92**, 251802 (2004).
[8] H. Albrecht *et al.* (ARGUS Collaboration), Phys. Lett. B **324**, 249 (1994).
[9] J. Bartelt *et al.* (CLEO Collaboration), Phys. Rev. Lett. **71**, 1680 (1993).
[10] P. Abreu *et al.* (DELPHI Collaboration), Z. Phys. C **74**, 19 (1997).
[11] G. Abbiendi *et al.* (OPAL Collaboration), Phys. Lett. B **493**, 266 (2000).
[12] Throughout the paper the momentum, energy and direction of all particles are computed in the e^+e^- rest frame.
[13] M. Artuso *et al.* (CLEO Collaboration), Phys. Rev. Lett. **80**, 3193 (1998).
[14] S. Eidelman *et al.* (Particle Data Group), Phys. Lett. B **592**, 1 (2004).
[15] Heavy Flavor Averaging Group, http://www.slac.stanford.edu/xorg/hfag/
[16] P. Robbe, Ph.D. thesis, 2002. See the Web page: https://oraweb.slac.stanford.edu:8080/pls/slacquery/bbrdownload/these.ps.gz?P_FRAME=DEST&P_DOC_ID=5319
[17] B. Aubert *et al.* (*BABAR* Collaboration), Phys. Rev. Lett. **88**, 221803 (2002).
[18] B. Aubert *et al.*, (*BABAR* Collaboration), Phys. Rev. D **67**, 072002 (2003).
[19] B. Aubert *et al.* (*BABAR* Collaboration), Phys. Rev. Lett. **87**, 201803 (2001).
[20] B. Aubert *et al.* (*BABAR* Collaboration), Phys. Rev. Lett. **88**, 221802 (2002).